Vol 461|22 October 2009|doi:10.1038/nature08447

LETTERS

Atmospheric carbon dioxide through the Eocene–Oligocene climate transition

Paul N. Pearson[1], Gavin L. Foster[2] & Bridget S. Wade[3]

Geological and geochemical evidence[1–3] indicates that the Antarctic ice sheet formed during the Eocene–Oligocene transition[4], 33.5–34.0 million years ago. Modelling studies[5,6] suggest that such ice-sheet formation might have been triggered when atmospheric carbon dioxide levels ($p_{CO_2}^{atm}$) fell below a critical threshold of ~750 p.p.m.v., but the timing and magnitude of $p_{CO_2}^{atm}$ relative to the evolution of the ice sheet has remained unclear. Here we use the boron isotope pH proxy[7,8] on exceptionally well-preserved carbonate microfossils from a recently discovered geological section in Tanzania[9,10] to estimate $p_{CO_2}^{atm}$ before, during and after the climate transition. Our data suggest that a reduction in $p_{CO_2}^{atm}$ occurred before the main phase of ice growth, followed by a sharp recovery to pre-transition values and then a more gradual decline. During maximum ice-sheet growth, $p_{CO_2}^{atm}$ was between ~450 and ~1,500 p.p.m.v., with a central estimate of ~760 p.p.m.v. The ice cap survived the period of $p_{CO_2}^{atm}$ recovery, although possibly with some reduction in its volume, implying (as models predict[11]) a nonlinear response to climate forcing during melting. Overall, our results confirm the central role of declining $p_{CO_2}^{atm}$ in the development of the Antarctic ice sheet (in broad agreement with carbon cycle modelling[12]) and help to constrain mechanisms and feedbacks associated with the Earth's biggest climate switch of the past 65 Myr.

The principal geochemical fingerprint of the Eocene–Oligocene transition (EOT) is an approximately +1.5‰ 'shift' towards more positive values of the oxygen isotope ratio of deep-sea carbonates between ~34.0 and 33.5 million years (Myr) ago, the last part of which is a prominent 'step' of about +0.5‰ at about 33.5 Myr ago[1,13,14]. The isotope shift corresponds to an extended period of global climatic disruption, widespread extinction and biogeographic reorganization[4,10]. Recent evidence[15,16] suggests that the first phase of the isotope shift was caused mainly by global cooling, with a little ice growth, while the end step was a geologically rapid phase of ice growth of less than 40,000 years (<40 kyr) with a smaller component of deep-sea cooling. The step occurred at a time when Earth's orbital parameters favoured ice-sheet growth[14,17] and was probably accelerated by positive feedbacks as a massive high-albedo ice cap was assembled[5,6]. At this point an 'ice-house' climate mode characterized by pronounced orbitally paced climate cycles was initiated[17]. The early Oligocene world was, nevertheless, warmer than today, with no evidence for sustained continental ice caps in the northern hemisphere, and possibly West Antarctica, until much later[2,6,18].

It is crucial for better prediction of future climate change to establish the level of radiative forcing through the EOT[3,19]. A variety of $p_{CO_2}^{atm}$ proxies through the Cenozoic era[19] suggest that values of >1,000 parts per million by volume (p.p.m.v.) were common in the Palaeocene and Eocene epochs, declining to near-modern levels by the early Miocene epoch (~23 Myr ago), but there is little agreement in detail between proxies and few data exist through the critical interval. The most detailed available record is from alkenone-based estimates[20], but even in that record there are no data from the EOT.

Here we used boron isotope ($\delta^{11}B$) analysis of the carbonate shells of upper-ocean planktonic foraminifera to establish palaeo-surface ocean pH (refs 7, 8) from which we infer the dissolved CO_2 concentration, $[CO_2]_{aq}$. In oligotrophic locations, $[CO_2]_{aq}$ is in approximate equilibrium with $p_{CO_2}^{atm}$. The main uncertainties are the value for the boron isotope ratio of seawater ($\delta^{11}B_{sw}$), sea surface temperature, and the requirement to estimate one other parameter of the carbonate system (for example, total alkalinity, $[CO_3^{2-}]$). We used estimates of $\delta^{11}B_{sw}$ from boron cycle modelling[21,22] and a two-box model to estimate $[CO_3^{2-}]$ changes in both surface and deep waters associated with the substantial stepwise changes in the oceanic calcite compensation depth[14,23] through the climate transition. Sea surface temperature estimates were made using Mg/Ca measurements on the same shells used for analysing $\delta^{11}B$, supported by $\delta^{18}O$ and organic temperature proxy measurements[10].

Geological sections with well-preserved planktonic foraminifera across the climate transition are rare. We recovered a suitable section from Tanzania in boreholes in the Kilwa Group, a bathyal outer shelf/slope deposit with oligotrophic open-ocean conditions[9,10]. Foraminifer shells are excellently preserved owing to the relatively impermeable clay

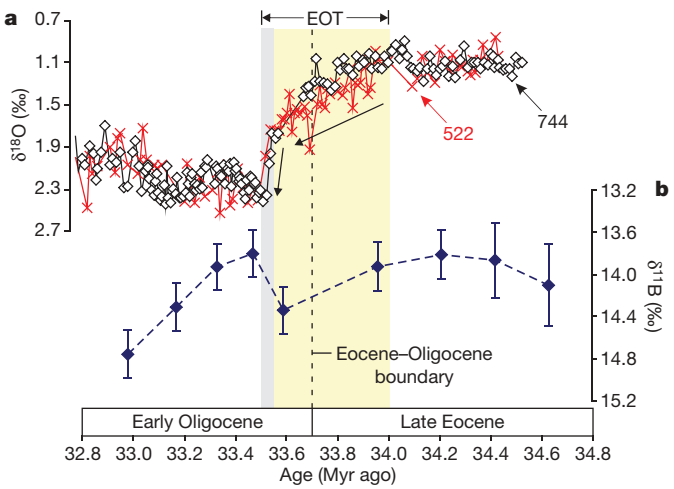

Figure 1 | Deep-sea oxygen isotope records across the EOT compared with boron isotopes from Tanzania. a, Deep-sea oxygen isotope records of benthic foraminifera from ODP sites 522 (red crosses) and 744 (black diamonds; ref. 13). Arrows indicate the 'shift' and 'step' in the isotope records referred to in the text. **b,** Boron isotope ratios of *Turborotalia ampliapertura* (212–250 μm), error bars reflect long-term analytical reproducibility or internal precision, whichever is larger (at 95% confidence).

[1]School of Earth and Ocean Sciences, Cardiff University, Cardiff CF10 3YE, UK. [2]Bristol Isotope Group, Department of Earth Sciences, University of Bristol, Bristol BS8 1RJ, UK. [3]Department of Geology and Geophysics, Texas A&M University, College Station, Texas 77843-3115, USA.

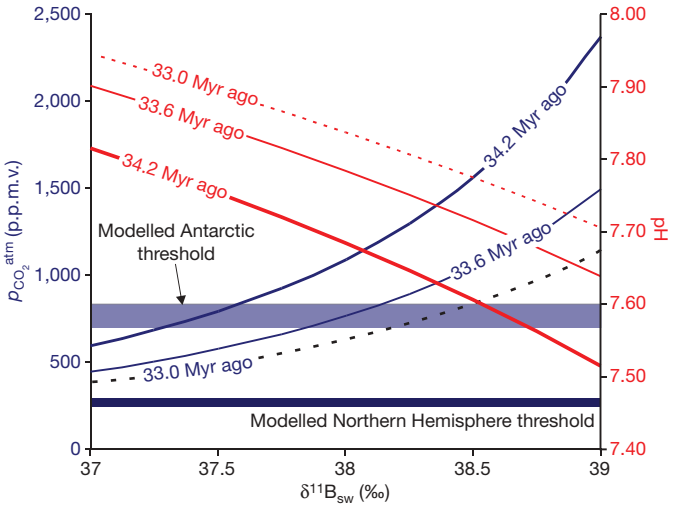

Figure 2 | Sensitivity of pH and atmospheric carbon dioxide estimates to $\delta^{11}B$ for sea water, with modelled atmospheric p_{CO_2} thresholds for ice growth. Blue lines show reconstructed $p_{CO_2}^{atm}$ for three time intervals. Thresholds for glaciation in the northern and southern hemispheres are from refs 5 and 6. Red lines show reconstructed pH values for the three time intervals. pH is reported on the total pH scale.

facies and shallow maximum burial depth of the deposit[10]. The section has already produced records of $\delta^{18}O$ (refs 10, 24) and Mg/Ca (ref. 15) through the EOT. We analysed nine samples spanning a period of ~1.6 Myr, with an average sample spacing of ~200 kyr. Measurements were made on shells of the non-symbiotic upper-ocean-dwelling foraminifer *Turborotalia ampliapertura*.

All boron isotope results are in the range $\delta^{11}B = 14.2 \pm 0.5$ (Supplementary Information and Fig. 1). Boron has a residence time in sea water (10–20 Myr)[21] sufficiently long that $\delta^{11}B_{sw}$ is unlikely to have changed significantly within the time window of our study. Because the $\delta^{11}B$ of foraminifer calcite is positively correlated with pH (refs 7, 8), which is in turn negatively correlated with $[CO_2]_{aq}$, the temporal pattern in $\delta^{11}B$ establishes a qualitative history of $p_{CO_2}^{atm}$ evolution regardless of the further assumptions we take in reconstructing absolute values. Our data show a significant increase in $\delta^{11}B$ in the period of global cooling before the main step in the oxygen isotope record indicating a decline in $p_{CO_2}^{atm}$, followed by a recovery to approximately pre-excursion values, and then further subsequent $\delta^{11}B$ increase (and $p_{CO_2}^{atm}$ decline; Fig. 1).

Geochemical models of the boron cycle[21,22] agree that $\delta^{11}B_{sw}$ was probably in the range +37 to +39‰ during this time interval. Figure 2 illustrates the sensitivity of our critical pH and $p_{CO_2}^{atm}$ estimates before, during and after the EOT to this range in seawater isotopic composition. The central $p_{CO_2}^{atm}$ estimate of ~760 p.p.m.v. at 33.6 Myr ago (where $\delta^{11}B_{sw} = 38.0$) is close to the range identified by ice-sheet models as the 'threshold' for Antarctic ice sheet growth (700–840 p.p.m.v.)[5,6], but we cannot rule out a value as low as ~450 p.p.m.v. or as high as ~1,500 p.p.m.v.. Even this wide range is useful, because 450 p.p.m.v. is nearly twice the modelled threshold value for Northern Hemisphere continental glaciation[6], supporting the contention that Oligocene glaciation was most probably unipolar[6]; and values much higher than 1,500 p.p.m.v. have been used in models of late Eocene climate[25]. Improvements in reconstructing $\delta^{11}B_{sw}$ are clearly required to refine our absolute estimates of $p_{CO_2}^{atm}$.

Using the central estimate in which $\delta^{11}B_{sw} = 38.0$‰ (ref. 21), the data indicate a significant increase in pH from ~7.7 to ~7.8 across

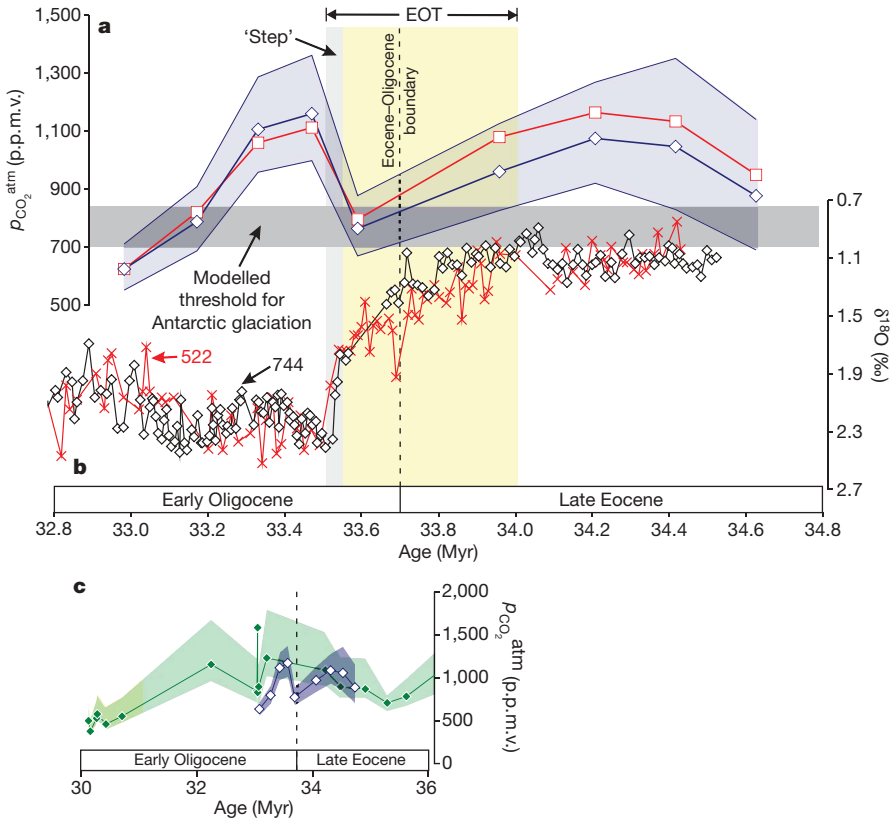

Figure 3 | Reconstructed $p_{CO_2}^{atm}$ compared with the deep-sea benthic foraminiferal stable isotope record. **a**, $p_{CO_2}^{atm}$ (± uncertainty from $\delta^{11}B$ measurements at 95% confidence). Blue symbols are calculated using modelled $[CO_3^{2-}]$ changes based on varying calcite compensation depth; red symbols are for constant $[CO_3^{2-}]$. The grey band is the threshold for Antarctic glaciation[5,6]. **b**, Deep-sea oxygen isotopes from DSDP site 522 (red crosses) and ODP site 744 (black diamonds; ref. 13). **c**, Alkenone proxy estimates (green symbols with green shaded band for maximum and minimum; ref. 20) and $\delta^{11}B$ proxy measurements (this study; colouring as in **a**).

the EOT that equates to a reduction in $p_{CO_2}^{atm}$ from ~1,100 p.p.m.v. to ~760 p.p.m.v. over the extended shift in the $\delta^{18}O$ curve, albeit with a large uncertainty (Fig. 3). A significant rise in $p_{CO_2}^{atm}$ to ~1,150 p.p.m.v. occurred after the main step in the $\delta^{18}O$ record, which was followed by further reductions to ~625 p.p.m.v. over the next 500 kyr. These $p_{CO_2}^{atm}$ estimates are in broad agreement with the alkenone proxy-derived estimates[20] (Fig. 3c) but add more detail, including the inferred $p_{CO_2}^{atm}$ decline before the $\delta^{18}O$ step and the sharp increase afterwards.

Cooling in the early phases of the EOT was associated with some ice growth[15,16], which models[5,6] and geomorphological observations[26] suggest was probably in isolated regions of Antarctica. The decline in $p_{CO_2}^{atm}$ detected in our study may have contributed to global cooling and preconditioned the system for explosive ice sheet growth at the time of the $\delta^{18}O$ step (~33.5 Myr ago) when orbital parameters were favourable[5,14]. The data indicate that once established, the Antarctic ice sheet withstood an increase in $p_{CO_2}^{atm}$ to levels that were similar to or slightly higher than before the climate transition. This hysteresis effect[11] occurs because the bright surface of the ice cap reflects more sunlight, and once an ice cap has formed, melting at its margin is compensated by flow from the cold, high altitude interior. Details in the $\delta^{18}O$ record from ODP site 744 (Fig. 3) suggest a slight rebound towards more negative values between about 33.5 and 33.3 Myr ago that could indicate partial melt-back of the ice cap and/or warming during this time of relatively high $p_{CO_2}^{atm}$. However, we note that this feature is not obvious in all $\delta^{18}O$ records through this interval[13,14].

Recent carbon cycle modelling[12] has used constraints provided by the stepwise fall in the calcite compensation depth[14,23] and observed deep-sea carbon isotope excursions[13,14] to explore a variety of possible feedbacks in the global carbon cycle during the EOT. The model preferred in ref. 12 involves a permanent increase in the ratio of calcium carbonate buried in deep-water environments compared with shallow seas as a consequence of the glacioeustatic sea-level fall. This scenario predicts a short-lived $p_{CO_2}^{atm}$ drop of ~300 p.p.m.v. over the transition, followed by a rebound to levels slightly higher than before the event, which is similar to the $p_{CO_2}^{atm}$ evolution suggested by our data. However, our study indicates that $p_{CO_2}^{atm}$ recovered more rapidly (within ~50 kyr) after the step in the $\delta^{18}O$ record than in the most favoured model of ref. 12 (~500 kyr). Moreover, the initial $p_{CO_2}^{atm}$ decline that we observe is associated with the long shift in the $\delta^{18}O$ record, which appears to have had only a relatively small component of ice growth[15,16], and hence would not have been associated with the maximum sea-level fall. A combination of several mechanisms, some of which are explored in ref. 12, is therefore needed to fit the additional constraint provided by our $p_{CO_2}^{atm}$ record. This may include release of organic carbon from geological reservoirs, changes in ocean productivity and circulation patterns, and variations in rock weathering rates[12,27,28].

The possible roles of declining greenhouse-gas forcing and tectonic gateway effects in promoting Antarctic glaciation across the Eocene–Oligocene boundary have been debated for decades[1,2,4]. Recent studies point to a consensus that ice growth followed an extended period of global cooling across continents[18,26] and in the oceans in shallow[15,16] and deep[13,14] water and in high[18,25,26] and low[15,16,25] latitudes. This strongly suggests that the primary cause was a diminishing greenhouse effect[25]. Although greenhouse gases other than CO_2 (for which there are no proxies) may have contributed, changing $p_{CO_2}^{atm}$ is likely to have had the greatest forcing[19]. Ours is the first proxy-based study to confirm a substantial $p_{CO_2}^{atm}$ decline during the climate transition. We also find a sharp $p_{CO_2}^{atm}$ increase after maximum ice growth as the global carbon cycle adjusted to the presence of a large ice cap and there was a nonlinear hysteresis effect as the ice cap withstood this transient $p_{CO_2}^{atm}$ rise. This study reaffirms the links between cryosphere development and atmospheric carbon dioxide levels at the largest and most important climatic tipping point of the last 65 million years.

METHODS SUMMARY

Foraminiferal samples were separated from 50-cm core segments from Tanzania Drilling Project sites 12 and 17 (ref. 9). The composite age model for these sites[10] is on the timescale of ref. 29. Foraminiferal calcite is exceptionally well-preserved and between 300 and 1,000 tests of *Turborotalia ampliapertura* (212–250 μm) were separated for each boron isotope analysis. Trace element and boron isotope analyses were carried out following ref. 8. Trace element and isotopic data are listed in the Supplementary Information. The pH is calculated from $\delta^{11}B$ using tandem Mg/Ca-derived temperatures and following ref. 8.

The second parameter of the carbonate system required to estimate $p_{CO_2}^{atm}$ is calculated for each sample from the evolution of the calcite compensation depth over the EOT, using a simple two-box model and $CaCO_3$ mass accumulation rate in the equatorial Pacific[14,23]. In the deep box (deep ocean) at the saturation depth (assumed to be approximated by the calcite compensation depth), $[CO_3^{2-}]$ equals $[CO_3^{2-}]$ at saturation. We assume a constant $[CO_3^{2-}]$ gradient between the deep box and upper box (surface ocean) of ~72 μmol mol^{-1} such that at 32.98 Myr ago (post-EOT) the surface water is 6.5 times oversaturated, the same as the pre-industrial western Indian Ocean[30]. By combining our pH estimate from $\delta^{11}B$ with this estimate of $[CO_3^{2-}]_{surface}$ we can calculate $[CO_2]_{aq}$ and thus $p_{CO_2}^{atm}$ using Henry's Law. Changing this gradient by ±25% or changing the depth of the calcite compensation depth by ±500 m does not alter our $p_{CO_2}^{atm}$ record beyond the uncertainty imposed by the measurement uncertainty in $\delta^{11}B$. Keeping $[CO_3^{2-}]_{surface}$ constant at post-EOT values also does not greatly influence our $p_{CO_2}^{atm}$ record (Fig. 3). This implies that our assumptions regarding this second parameter of the carbonate system are of secondary importance and the $p_{CO_2}^{atm}$ evolution we reconstruct is driven predominantly by the measured $\delta^{11}B$.

Full Methods and any associated references are available in the online version of the paper at www.nature.com/nature.

Received 18 May; accepted 21 August 2009.
Published online 13 September 2009.

1. Kennett, J. P. & Shackleton, N. J. Oxygen isotopic evidence for the initiation of the psychrosphere 38 Myr ago. *Nature* **260,** 513–515 (1976).
2. Barrett, P. in *Developments in Earth and Environmental Sciences* (eds Florindo, F. & Siegert, M.) Vol. 8, 34–83 (Elsevier, 2009).
3. Zachos, J. C., Dickens, G. R. & Zeebe, R. E. An early Cenozoic perspective on greenhouse warming and carbon-cycle dynamics. *Nature* **451,** 279–283 (2008).
4. Coxall, H. K. & Pearson, P. N. in *Deep-time Perspectives on Climate Change: Marrying the Signal from Computer Models and Biological Proxies* (eds Williams, M. *et al.*) 351–387 (The Micropalaeontological Society, Special Publications, The Geological Society, London, 2007).
5. Deconto, R. M. & Pollard, D. Rapid Cenozoic glaciation of Antarctica triggered by declining atmospheric CO_2. *Nature* **421,** 245–249 (2003).
6. Deconto, R. M. *et al.* Thresholds for Cenozoic bipolar glaciation. *Nature* **455,** 652–656 (2008).
7. Hemming, N. G. & Hanson, G. N. Boron isotope composition and concentration in modern marine carbonates. *Geochim. Cosmochim. Acta* **59,** 371–379 (1992).
8. Foster, G. L. Seawater pH, pCO_2 and $[CO_3^{2-}]$ variations in the Caribbean Sea over the last 130 kyr: a boron isotope and B/Ca study of planktic foraminifera. *Earth Planet. Sci. Lett.* **271,** 254–266 (2008).
9. Nicholas, C. J. *et al.* Stratigraphy and sedimentology of the Upper Cretaceous to Paleogene Kilwa Group, southern coastal Tanzania. *J. Afr. Earth Sci.* **45,** 431–466 (2006).
10. Pearson, P. N. *et al.* Extinction and environmental change across the Eocene–Oligocene boundary in Tanzania. *Geology* **36,** 179–182 (2008).
11. Pollard, D. & Deconto, R. M. Hysteresis in Cenozoic Antarctic ice-sheet variations. *Global Planet. Change* **45,** 9–21 (2005).
12. Merico, A., Tyrell, T. & Wilson, P. A. Eocene/Oligocene ocean de-acidification linked to Antarctic sea-level fall. *Nature* **452,** 979–983 (2008).
13. Zachos, J. C., Quinn, T. M. & Salamy, K. A. High resolution (10^4 years) deep-sea foraminiferal stable isotope records of the Eocene–Oligocene climate transition. *Paleoceanography* **11,** 251–256 (1996).
14. Coxall, H. K., Wilson, P. A., Pälike, H., Lear, C. H. & Backman, J. Rapid stepwise onset of Antarctic glaciation and deeper calcite compensation in the Pacific Ocean. *Nature* **433,** 53–57 (2003).
15. Lear, C. H., Bailey, T. R., Pearson, P. N., Coxall, H. K. & Rosenthal, Y. Cooling and ice growth across the Eocene–Oligocene transition. *Geology* **36,** 251–254 (2008).
16. Katz, M. E. *et al.* Stepwise transition from the Eocene greenhouse to the Oligocene icehouse. *Nature Geosci.* **1,** 329–334 (2008).
17. Pälike, H. *et al.* The heartbeat of the Oligocene climate system. *Science* **314,** 1894–1898 (2006).
18. Eldrett, J. S., Greenwood, D. R., Harding, I. C. & Huber, M. Increased seasonality through the Eocene to Oligocene transition in northern high latitudes. *Nature* **459,** 969–974 (2009).
19. Hansen, J. *et al.* Target atmospheric CO_2: Where should humanity aim? *Open Atmos. Sci. J.* **2,** 217–231 (2008).

20. Pagani, M., Zachos, J. C., Freeman, K. H., Tipple, B. & Bohaty, S. M. Marked decline in atmospheric carbon dioxide concentrations during the Paleogene. *Science* **309,** 600–603 (2005).
21. Lemarchand, D., Gaillardet, J., Lewin, É. & Allègre, C. J. Boron isotope systematics in large rivers: implications for the marine boron budget and paleo-pH reconstruction over the Cenozoic. *Chem. Geol.* **190,** 123–140 (2002).
22. Simon, L., Lecuyer, C., Marechal, C. & Coltice, N. Modelling the geochemical cycle of boron: implications for the long-term $\delta^{11}B$ evolution of seawater and oceanic crust. *Chem. Geol.* **225,** 61–76 (2006).
23. Rea, D. K. & Lyle, M. W. Paleogene calcite compensation depth in the eastern subtropical Pacific: answers and questions. *Paleoceanography* **20,** PA1012, doi:10.1029/2004PA001064 (2005).
24. Wade, B. S. & Pearson, P. N. Planktonic foraminiferal turnover, diversity fluctuations and geochemical signals across the Eocene/Oligocene boundary in Tanzania. *Mar. Micropal.* **68,** 244–255 (2008).
25. Liu, Z. *et al.* Global cooling during the Eocene–Oligocene climate transition. *Science* **323,** 1187–1190 (2009).
26. Bo, S. *et al.* The Gamburtsev mountains and the origin and early evolution of the Antarctic ice sheet. *Nature* **459,** 690–693 (2009).
27. Salamy, K. A. & Zachos, J. C. Latest Eocene–early Oligocene climate change and Southern Ocean fertility: inferences from sediment accumulation and stable isotope data. *Palaeogeogr. Palaeoclimatol. Palaeoecol.* **145,** 61–77 (1999).
28. Zachos, J. C. & Kump, L. R. Carbon cycle feedbacks and the initiation of Antarctic glaciation in the earliest Oligocene. *Glob. Planet. Change* **47,** 51–66 (2005).
29. Cande, S. C. & Kent, D. V. Revised calibration of the geomagnetic polarity timescale for the Late Cretaceous and Cenozoic. *J. Geophys. Res.* **100,** 6093–6095 (1995).
30. Key, R. M. *et al.* A global ocean carbon climatology: results from Global Data Analysis Project (GLODAP). *Glob. Biogeochem. Cycles* **18,** GB4031, doi:10.1029/2004GB002247 (2004).

Supplementary Information is linked to the online version of the paper at www.nature.com/nature.

Acknowledgements This work was supported by NERC grants to P.N.P., B.S.W. and G.L.F. We thank the Tanzania Petroleum Development Corporation, the Tanzania Commission for Science and Technology and the Tanzania Drilling Project field team for support. We are grateful to T. Elliott for discussions.

Author Contributions P.N.P. led the study and fieldwork, prepared foraminifer samples for isotope analysis and wrote the initial draft. G.L.F. conducted all isotope and trace element analyses and calculations and drafted the figures. B.S.W. contributed to fieldwork and prepared foraminifer samples for trace element analyses. All authors contributed to the final text.

Author Information Reprints and permissions information is available at www.nature.com/reprints. Correspondence and requests for materials should be addressed to P.N.P. (pearsonp@cardiff.ac.uk).

METHODS

Sample preparation. Foraminiferal tests with extensive visible pyrite contamination were separated before crushing. All samples were crushed and cleaned following the method in ref. 31 except that we did not carry out a reductive step and samples were dissolved in 0.1 M HNO_3 with centrifuging shortly after dissolution to remove any insoluble residue. Analysis of the residue after dissolution and repeat dissolutions of the separated pyrite-rich subsamples indicate that pyrite does not contain significant Mg or B and the samples can be considered free of pyrite contamination, provided the measured Fe/Ca was $<3{,}000\ \mu mol\ mol^{-1}$. The majority of samples here have Fe/Ca $<1{,}000\ \mu mol\ mol^{-1}$.

Trace element analysis and temperature estimates. The samples of *Dentoglobigerina* cf. *D. tapuriensis*, *Hantkenina* spp. and a small aliquot (10%) of the *T. ampliapertura* selected for isotope analysis were analysed for trace element composition using a ThermoFisher Scientific Element 2 at the University of Bristol following the methodology outlined in ref. 8. Trace element data are tabulated in Supplementary Table 2. This tandem trace element analysis allowed an assessment of cleaning efficiency and Mg/Ca ratios required to estimate temperature (Supplementary Table 2). The long-term reproducibility of our Mg/Ca ratios is around 2% at 95% confidence, based on repeat measurements of three consistency standards over the duration of this study. Sea water temperatures were calculated using a generic Mg/Ca temperature equation[32] and assuming a seawater Mg/Ca ratio of $4.3\ mol\ mol^{-1}$ (ref. 33). Sea surface temperatures are $\sim$2 °C warmer than the temperature we calculate here for *T. ampliapertura*[15,24]. Our temperature evolution across the EOT is therefore in good agreement with a number of recent studies[15,16,25]. The similarity between *Hantkenina* spp. and *T. ampliapertura* support our assignment of the latter as an upper-ocean dweller (originally based on $\delta^{18}O$ and $\delta^{13}C$ measurements[24]). The Mg/Ca ratios of *Dentoglobigerina* cf. *D. tapuriensis* show little change across the EOT, and in all cases this species records lower temperatures owing to its deeper habitat[24].

Boron isotope analysis and palaeo-pH. Boron was separated from the dissolved samples of *T. ampliapertura* using boron-specific anion exchange resin[8]. The boron isotopic composition was determined using a sample-standard bracketing routine on a ThermoFisher Scientific Neptune multicollector inductively coupled plasma mass spectrometer (MC-ICPMS) at the University of Bristol[8]. The full boron isotope data set is shown in Supplementary Table 1 and our long-term reproducibility is ±0.22‰ at 95% confidence, based on repeat total procedural replicates of similar-sized samples of our in-house carbonate standards ($\delta^{11}B = 24.67 \pm 0.22$‰; 2 s.d., $n = 11$ and $\delta^{11}B = 23.93 \pm 0.22$‰; 2 s.d., $n = 18$).

When measured by MC-ICPMS, and using the isotopic fractionation factor of ref. 34, the $\delta^{11}B$ of planktonic foraminiferal carbonate is very close (<0.8‰) to the $\delta^{11}B$ of $B(OH)_4^-$ ion in sea water[8], which is itself pH-dependent[7]. The following equation, modified from ref. 7, can thus be used to estimate pH on the total scale:

$$pH = pK^*_{boric} - \log\left[-\frac{\delta^{11}B_{sw} - \delta^{11}B_{foram}}{\delta^{11}B_{sw} - (1.0272\delta^{11}B_{foram}) - 27.2}\right]$$

where pK^*_{boric} is $-\log_{10}$ of the stoichiometric equilibrium constant for boric acid[35] at the *in situ* temperature and salinity (from Mg/Ca temperature and assumed to be 35 practical salinity units, p.s.u., respectively), $\delta^{11}B_{sw}$ is the isotopic composition of sea water ($\delta^{11}B = 37$–39‰), and $\delta^{11}B_{foram}$ is the measured isotopic composition of the foraminifer *T. ampliapertura*. In studies of modern planktonic foraminifera intra-species $\delta^{11}B$ differences are largely due to different depth habitats, and small offsets from the $\delta^{11}B$ of $B(OH)_4^-$ relate to symbiont activity and foraminiferal respiration (ref. 8 and references therein). *T. ampliapertura* is an extinct surface-dwelling non-spinose foraminifer so here we assume that there is no offset between the measured $\delta^{11}B$ of *T. ampliapertura* and $B(OH)_4^-$ in sea water and that the calculated pH is that of the mixed layer. This assumption does not affect our reconstructions unduly because it is of secondary magnitude given the range of $\delta^{11}B$ of sea water we use and is likely to be constant between samples. Uncertainties in pH for a given $\delta^{11}B_{sw}$ are dominated by measurement uncertainties in the $\delta^{11}B$. We note that our $\delta^{11}B$ data are not directly comparable with earlier Cenozoic boron isotope measurements[36] because significant inter-laboratory bias exists[8].

The second carbonate system parameter. To estimate $p_{CO_2}{}^{atm}$ from $\delta^{11}B$-derived pH, a second parameter of the carbonate system is needed. We use a simple two-box model to accomplish this. The $[Ca]_{sw}$ concentration of the Eocene ocean has been estimated from fluid inclusion studies to be in the range 12 to 20 $mmol\ kg^{-1}$ (ref. 37) and following previous studies we use the central value of 17 $mmol\ kg^{-1}$ (refs 37, 38). At saturation $[CO_3{}^{2-}] = K_{sp}/[Ca]$, where K_{sp} is the solubility product of $CaCO_3$ adjusted for the influence of changing [Mg] and [Ca] of sea water (following ref. 38). In the lower box of our model (which represents the deep ocean) we alter $[CO_3{}^{2-}]$ until the saturation horizon (the depth separating waters oversaturated with respect to $CaCO_3$ from waters undersaturated below) is at 4 km—a depth that is approximately that of the calcium carbonate compensation depth in the Pacific Ocean after the EOT[23]. The $[CO_3{}^{2-}]$ is then altered through the EOT, guided by the $CaCO_3$ mass accumulation rate at ODP site 1218 (ref. 14). Working back through time we initially shoal the calcite compensation depth to 3.5 km, then deepen it to 4.5 km coincident with the maximum in $\delta^{18}O$ and $CaCO_3$ mass accumulation rate at ODP site 1218 (refs 14, 23). Then, in two steps we decrease the depth to 2.5 km, reflecting the minimum in $CaCO_3$ mass accumulation rate at ODP site 1218 at $\sim$34.0 Myr ago. We then deepen and hold the calcite compensation depth at 3 km until $\sim$34.6 Myr ago. To determine the $[CO_3{}^{2-}]$ in the upper box (the surface ocean) we assume a constant gradient in $[CO_3{}^{2-}]$ of $\sim 72\ \mu mol\ mol^{-1}$ between the two boxes. The magnitude of this gradient is fixed so that at 32.98 Myr ago the degree of $CaCO_3$ oversaturation in the surface box is similar to the pre-industrial value in the western Indian Ocean (6.5 times oversaturated; calculated from ref. 30).

By combining our pH estimate from $\delta^{11}B$ with this estimate of $[CO_3{}^{2-}]$ we can calculate $[CO_2]_{aq}$ and thus $p_{CO_2}{}^{atm}$ using Henry's Law. For the detail of these calculations see ref. 8 and references therein. Following ref. 38 we also account in these calculations for the effect of changing [Mg] and [Ca] of sea water on the carbonic acid dissociation constants K_1 and K_2. Although large changes in our assumed $[CO_3{}^{2-}]$ gradient are unlikely[38], we note that changing its magnitude by ±25% or changing the depth of the calcite compensation depth by ±500 m does not alter our $p_{CO_2}{}^{atm}$ record beyond the uncertainty imposed by the measurement uncertainty in $\delta^{11}B$ for a given $\delta^{11}B_{sw}$. Also, although a temperature and salinity reconstruction is required to reconstruct pH, the resultant record is relatively insensitive to inaccuracies in these parameters. For example, a 2 °C temperature change alters $p_{CO_2}{}^{atm}$ by <50 p.p.m.v. and a 2 p.s.u. salinity change alters $p_{CO_2}{}^{atm}$ by <10 p.p.m.v.

31. Barker, S., Greaves, M. & Elderfield, H. A study of cleaning procedures used for foraminiferal Mg/Ca paleothermometry. *Geochem. Geophys. Geosyst.* **4**, 8407, doi:10.10292003GC000559 (2003).
32. Anand, P., Elderfield, H. & Conte, M. H. Calibration of Mg/Ca thermometry in planktonic foraminifera from a sediment trap time series. *Paleoceanography* **18**, 1050, doi:10.1029/2002PA000846 (2003).
33. Wilkinson, B. H. & Algeo, T. J. Sedimentary carbonate record of calcium-magnesium cycling at the Earth's surface. *Am. J. Sci.* **289**, 1158–1194 (1989).
34. Klochko, K., Kaufman, A. J., Yao, W., Berne, R. H. & Tossell, J. A. Experimental measurement of boron isotope fractionation in seawater. *Earth Planet. Sci. Lett.* **248**, 276–285 (2006).
35. Dickson, A. G. Thermodynamics of the dissociation of boric acid in synthetic seawater from 273.15 to 318.15 K. *Deep-Sea Res.* **37**, 755–766 (1990).
36. Pearson, P. N. & Palmer, M. R. Atmospheric carbon dioxide concentrations over the past 60 million years. *Nature* **406**, 695–699 (2000).
37. Horita, J., Zimmermann, H. & Holland, H. D. Chemical evolution of seawater during the Phanerozoic: implications from the record of marine evaporates. *Geochim. Cosmochim. Acta* **66**, 3733–3756 (2002).
38. Tyrrell, T. & Zeebe, R. E. History of carbonate ion concentration over the last 100 million years. *Geochim. Cosmochim. Acta* **68**, 3521–3534 (2004).